Macropixel Compressive Sensing Reconstruction of Spectral Images Sensed by Multispectral Filter Array-based Sensors

Yuri H. Mejia, Fernando A. Rojas, and Henry Arguello
Department of Systems Engineering and Computer Science
Universidad Industrial de Santander
Bucaramanga, Colombia
email: yuri.mejia@correo.uis.edu.co, frojas@uis.edu.co, henarfu@uis.edu.co

***Abstract*—Spectral images are 3 dimensional data cubes of spectral information from a two-dimensional spatial scene. Traditional acquisition of these data cubes includes complex architectures that involves the use of prisms, tunable filters, and tunable illumination. Technical progress has allowed developing MSFA-based sensors in order to extrapolate the reconstruction of more bands than RGB cameras. However, reconstructing the spectral images with traditional mathematical methods following a least squares or demosaicing approach is unfeasible. Recently compressive sensing technique has been developed that allows reconstructing signals with few measurements than the traditional methods by using the sparse representation of the underlying signal. It is possible to exploit the capabilities of MSFA-based sensors selecting measurements subsets to form macropixels that have spectral information of a single reconstructed pixel. The macropixel size selection leads to a variable reconstructed spatial resolution preserving the filters spectral resolution. This paper presents a model for spectral images reconstruction from macropixels formed with MSFA-based sensor measurements using the principle of compressive sampling. This model selects subsets of the macropixels measurements following a downsampling matrix operation, therefore a reconstruction model is formulated by directly reconstruct a spectral image with the spectral resolution given by the number of filters. To verify the effectiveness of the reconstruction model measurements of the MSFA-based sensor for real spectral images are simulated. An ensemble of random dichroic filters is used. The macropixel compressive sensing reconstruction approach and the traditional scheme reconstruction are compared.**

Keywords- spectral images; MSFA-based sensors; compressive sensing; macropixel.

I. INTRODUCTION

Spectral imaging involves the sensing of a scene where at every location of the image plane the spectral information is collected. Its applications are many and cover ocean research, food safety, geology, and medical demands. Some examples involve the characterization of phytoplankton in the ocean [1], quality evaluation in the area of food safety [2], plant stress assessment [3], characterization of different bacterial colonies [4], disease diagnosis, and image-guided surgery [5].

In some spectral imagers, the scene is beamsplit into the wavelength components for example using a prism assembly, and each of these images is captured in a separate detector array. In this method the sensing devices have significant size and weight disadvantages [6]. One of the most intuitive multispectral scanning techniques is the tunable filter, where a complete spectral image is produced after a sequence of exposures by capturing an image of one spectral band at time. For instance, the spectral image can be sensed by using a filter wheel where some optical filters are installed in a rotatory mechanical structure [7]. Most of the methods are related to scanning operations where multiple exposures are used causing motion artifacts.

On the contrary, some techniques use MSFA and collect multiple wavelength spectra from a single detector array [8]. Nowadays, optical coatings technologies have been miniaturized and optimized such that the creation of multi-patterned arrays of different optical filters, with traditional design and manufacturing methods, is allowed [6]. The optical coatings production methodology combines modern optical thin film deposition techniques with microlithographic procedures. This process enables micron-scale precision patterning of optical thin film dichroic coatings on a single substrate. A dichroic filter is an accurate color filter used to selectively pass light of a small range of wavelengths while reflecting other wavelengths.

Figure 1 shows a representation of a MSFA-based sensor that is a monochrome image sensor covering with a MSFA, each pixel in the sensor is measuring only some spectral components at a specific spatial location. Since there are only some wavelength elements available in each pixel, the missing wavelength elements must be estimated from the adjacent pixels. This process is called multispectral demosaicing, and in most cases is carried out depending on the specific acquisition process.

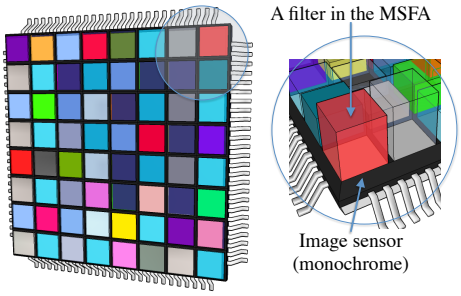

Figure 1. A MSFA-based sensor is illustrated.

For example, Miao et al. [9] generate a MSFA following a binary tree-based method, which starts from a checkerboard pattern. By recursively separating the original checkerboard, the algorithm generates the MSFA given the number of spectral bands and the probability of appearance of each band. Then, they design a demosaicing algorithm based on the same binary tree. Brauers and Aach [10] propose a MSFA that consists of color filter blocks of the

 ISBN: 978-1-61208-426-8

size 3×2 pixels, this configuration allows to use a fast bilinear interpolation with a reconstruction up to 6 spectral bands. Monno et al. [11] propose a five-band MSFA. In the pattern, the green-like channel is distributed as in the Bayer color filter array (CFA), and other channels are arranged following a binary-tree approach. For demosaicing an adaptive kernel can be estimated directly from the raw data. Common to these systems is that the MSFA design is application and number of bands dependent, which reach at most 6.

On the other hand, Compressive Sensing (CS) has emerged as a rising research area that allows the acquisition of signals at sampling rates below the Nyquist-criterion. In CS traditional sampling is substituted by measurements of random projections of the signal. The signals are then reconstructed by solving an l_1 and l_2 minimization problem in a basis where admits sparse representations. CS exploits the fact that hyperspectral images can be sparse in some basis representation.

Mathematically, a multispectral image $\mathbf{F}\in\Re^{N\times N\times L}$ in its vector representation $\boldsymbol{f}\in\Re^{M}$ with $M=N^2L$, can be expressed as $\boldsymbol{f}=\boldsymbol{\Psi\theta}$, where $\boldsymbol{\theta}$ is the coefficients sequence of S elements that represents $\boldsymbol{f}$, with $S<<M$, and $\boldsymbol{\Psi}$ is a representation basis. Here, $N\times N$ represents the spatial dimensions, and L the number of spectral bands in the data cube. Compressive sensing allows $\boldsymbol{f}$ recovering from m random projections when $m \geq S \log(M) << M$.

Assuming that the MSFA-based sensor performs a linear measurement process that calculate $m<<M$ internal products between $\boldsymbol{f}$ and a collection of vectors $\{\boldsymbol{H}_j\}_{j=1}^{m}$, as $y_i = \langle \boldsymbol{f}, \boldsymbol{H}_j \rangle$, then $\boldsymbol{y}=\mathbf{H}\boldsymbol{f}$, where the set of y_i projections form the vector $\boldsymbol{y}$ of m elements, $\mathbf{H}$ is the measurement matrix with dimensions $m\times M$, with H_j^T rows, and $\boldsymbol{f}$ is the original signal of size M. For recovering $\boldsymbol{f}$ from $\boldsymbol{y}$, there exist infinite solutions due to the size of $\boldsymbol{y}$ is much less than the size of $\boldsymbol{f}$.

Following the sparse representation of the signal and the MSFA-based sensor, measurements can be expressed as $\boldsymbol{y}=\mathbf{H}\boldsymbol{f}=\mathbf{H}\boldsymbol{\Psi\theta}=\mathbf{A}\boldsymbol{\theta}$, where $\mathbf{A}=\mathbf{H}\boldsymbol{\Psi}\in\Re^{m\times M}$ is the sensing matrix. This underdetermined equation system can be solved if it is satisfied that the measurement matrix $\mathbf{H}$ is incoherent with the sparse transformation $\boldsymbol{\Psi}$. It is possible to exploit the capabilities of MSFA-based sensors selecting measurements subsets to form macropixels that have spectral information of a single reconstructed pixel. That is, spectral information of a single pixel can be reconstructed based on macropixel measurements. The macropixel size selection leads to a variable reconstructed spatial resolution preserving the filters spectral resolution, reconstructing a spatial decimated data cube. This information can be used in applications requiring higher spectral than spatial image quality, also for a quick view of the scene, for example for purposes of transmission and communication applications

This paper presents a model for spectral images reconstruction from macropixels formed with MSFA-based sensor measurements using the principle of compressive sampling. This model selects subsets of the macropixels measurements following a downsampling matrix operation, therefore a reconstruction model is formulated by directly reconstruct a spectral image of variable spatial resolution. The maximum spatial resolution is limited by the detector resolution. The number of different filters limits the spectral resolution.

The data cube is then reconstructed as $\tilde{\boldsymbol{f}} = \boldsymbol{\Psi}\,(\underset{\boldsymbol{\theta}}{\operatorname{argmin}}\|\boldsymbol{y}-\mathbf{H}_S\boldsymbol{\Psi\theta}\|_2+\tau\|\theta\|_1)$, where $\boldsymbol{y}$ is the measurement selection, $\mathbf{H}_S$ is the measurement matrix defined as $\mathbf{H}_S=[(\mathbf{D}^0)^T\ldots(\mathbf{D}^{q^2-1})^T]^T\mathbf{H}$, where $\mathbf{D}^{\ell}$ is the ℓ^{th} downsampling matrix used for measurement selection, $\boldsymbol{\theta}$ is an S-sparse representation of a low resolution version of $\boldsymbol{f}$ on the basis $\boldsymbol{\Psi}$, and τ is a regularization constant.

The rest of this paper is organized as follows. Section II describes the mathematical model of the spectral image acquisition system using MSFA-based sensors. Section III describes the traditional demosaicing process. Section IV addresses the macropixel CS reconstruction approach. Section V describes the mathematical model of the dichroic filters. Section VI shows the simulation results. The conclusion closes the article.

II. SPECTRAL IMAGE ADQUISITION

To analyze the sensor-MSFA system its functions are modeled following the physical sensing phenomena for $L=6$ spectral bands and focusing in the j^{th}-slice in Figure 2. First, the MSFA $T(x, y, \lambda)$ modulates the spatial-spectral data cube $f_0(x, y, \lambda)$, resulting in the coded field $f_1(x, y, \lambda)$, where (x, y) are the spatial coordinates, and λ is the wavelength. Then the coded density impacts on the sensor.

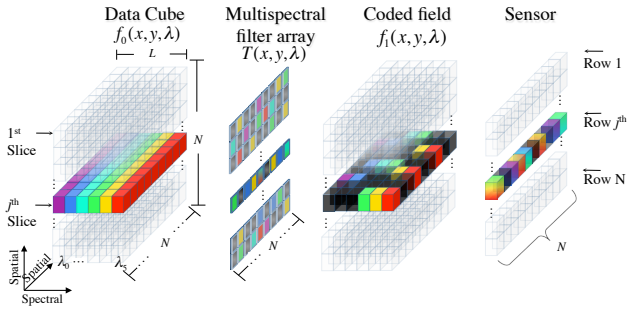

Figure 2. Sensing phenomena representation of the MSFA-based sensor. The j^{th} slice of the data cube is coded by a row of the MSFA.

The coded density integrated into the detector can be expressed as

$$f_2(x,y,\lambda) = \iint T(x',y',\lambda) f_1(x',y',\lambda) h(x'-x,y'-y)\,dx'dy', \qquad (1)$$

where $T(x',y',\lambda)$ is the transmission function representing the MSFA, and $h(x'-x,y'-y)$ is the optical response of the system.

Each pixel in the sensor is a discretized measurement. The source $f_0(x, y, \lambda)$ can be written in discrete form as $F_{i,j,k}$

where i and j index the spatial coordinates, and k determines the k^{th} spectral plane. Let $T_{i,j,k} \in \{0,1\}$ be the discretization of the MSFA.

Then, the discretized MSFA-based sensor measurements can be expressed as

$$Y_{i,j} = \sum_{k=0}^{L-1} F_{i,j,k} T_{i,j,k} + \omega_{i,j}, \qquad (2)$$

where $Y_{i,j}$ is the intensity at the $(i,j)^{\text{th}}$ position of the detector, i, j=0, 1, …, N-1, and the dimensions of the detector are $N \times N$. F is an $N \times N \times L$ spectral data cube, and $\omega_{i,j}$ is the white noise of the sensing system.

The measurements $Y_{i,j}$ in (2) can be written in matrix notation as

$$\boldsymbol{y} = \mathbf{H}\boldsymbol{f} + \boldsymbol{\omega}, \qquad (3)$$

where $\boldsymbol{y}$ is an N^2-long vector representation of $Y_{i,j}$, $\boldsymbol{f}$=vect([$\boldsymbol{f}_0$, …, $\boldsymbol{f}_{L-1}$]) is the vector representation of the data cube $\mathbf{F}$ where $\boldsymbol{f}_k$ is the vectorization of the k^{th} spectral band.

The output $\boldsymbol{y}$ in (3) can be extended as

$$\boldsymbol{y} = \underbrace{\left[\text{diag}(\mathbf{t}_0) \cdots \text{diag}(\mathbf{t}_{L-1})\right]}_{\mathbf{H}} \begin{bmatrix} \boldsymbol{f}_0 \\ \boldsymbol{f}_1 \\ \vdots \\ \boldsymbol{f}_{L-1} \end{bmatrix} + \omega, \qquad (4)$$

where $\mathbf{t}_k$ is the vectorization of the k^{th} MSFA spectral plane, diag($\mathbf{t}_k$) is an $N^2 \times N^2$ diagonal matrix whose entries are $\mathbf{t}_k$, more specifically $(\mathbf{t}_k)_i = T_{\lfloor i/N \rfloor, i-\lfloor i/N \rfloor N, k}$ for i=0, …, N^2-1. Figure 3 depicts a random MSFA based matrix $\mathbf{H}$ for N=6, and L=4. Colored squares represent unblocking light elements related to a specific wavelength.

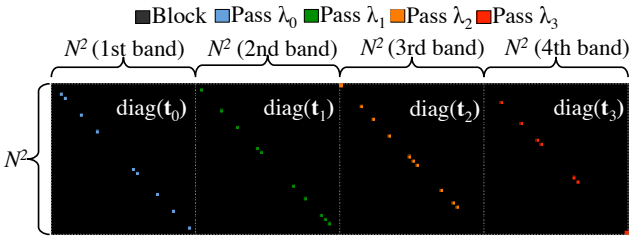

Figure 3. The matrix $\mathbf{H}$ is shown for N=6, and L=4. Colored squares represent unblocking light elements related to a specific wavelenght.

III. TRADITIONAL DEMOSAICING

Given the set of measurements $\boldsymbol{y}$ a traditional demosaicing algorithm estimates for each reconstructed pixel the intensities for all wavelength components. Common approach minimizes the linear mean square error between the measurements and the vector estimation multiplied by the sensing matrix, that is

$$\tilde{\boldsymbol{f}} = \arg\min_{\boldsymbol{f}} \left\| \boldsymbol{y} - \mathbf{H}\boldsymbol{f} \right\|_2, \qquad (5)$$

A closed-form solution to (5) is given by

$$\tilde{\boldsymbol{f}} = \left(\mathbf{H}^{\mathrm{T}}\mathbf{H}\right)^{-1}\mathbf{H}^{\mathrm{T}}\boldsymbol{y} = \mathbf{H}^{+}\boldsymbol{y}, \qquad (6)$$

where $\mathbf{H}^{+}$ is known as the pseudoinverse of $\mathbf{H}$, and $\mathbf{H}^{\mathrm{T}}$ is its transpose. For comparison purpose, this approach is implemented.

Also, for the spatial resolution variation of the data cube an average decimation matrix is applied to the reconstructed data cube. The variable q is defined as the macropixel side size; each macropixel in a spectral band is a block of dimensions $q \times q$ pixels, where the ratio N/q is an integer. The decimated reconstruction is given by $\tilde{\boldsymbol{f}}_q = \mathbf{D}\tilde{\boldsymbol{f}}$, where $\mathbf{D}$ does a block averaging of size $q \times q$ in each spectral band reducing the size of the vectorized reconstructed data cube to $\frac{N^2 L}{q^2} \times 1$. The spatial decimation matrix element-by-element can be expressed as:

$$\boldsymbol{D}_{i,j} = \begin{cases} \dfrac{1}{q^2}, & \text{if } i = \left\lfloor \dfrac{j}{q} \right\rfloor - \dfrac{N}{q}\left\lfloor \dfrac{j}{N} \right\rfloor + \dfrac{N}{q}\left\lfloor \dfrac{j}{qN} \right\rfloor, \\ 0, & \text{otherwise,} \end{cases} \qquad (7)$$

where $i = 0,1,\cdots, \dfrac{N^2 L}{q^2} - 1$, and j=0,1,…, N^2L-1.

IV. MACROPIXEL COMPRESSIVE SENSING RECONSTRUCTION

In this model, the macropixel definition is based on the assumption that $q \times q$ neighboring pixels, in an $N \times N \times L$ spectral image, could have a similar spectral response, Figure 4 illustrates this premise. Then, the macropixel, which is formed of $q \times q$ measurement pixels in the sensor, is taken as the spectral response of a single pixel for a decimated reconstruction. For instance, Figure 5 shows an example of the measurement selection for a macropixel side size of q=2. In total are taken q^2 subsets of measurements in a single shot of the MSFA-based sensor.

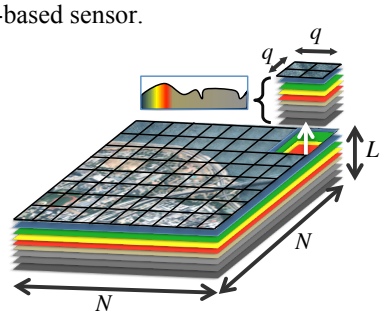

Figure 4. Illustration of the assumption that for $q \times q$ neighboring pixels, in a $N \times N \times L$ spectral image, the spectral response is simillar.

In the acquisition model, the matrix product between a downsampling matrix and the total sensor measurements forms each subset of measurements. More specifically, each subset is given by

$$\boldsymbol{y}^{\ell} = \mathbf{D}^{\ell}\mathbf{H}\boldsymbol{f}, \qquad (8)$$

where $\mathbf{D}^{\ell}$ does a downsampling in each $q \times q$ square of pixels for taken q^2 different subsets of the total measurements, and $\boldsymbol{y}^{\ell}$ is the ℓ^{th} subset of measurements where $\ell \in \{0, \cdots q^2 - 1\}$. Figure 5 shows an example of a subset measurement selection for q=2. Precisely, the function of the decimation matrix $\mathbf{D}^{\ell}$ is selecting in each $q \times q$ block of the measurements the ℓ^{th} -element for forming the ℓ^{th} -subset of

measurements. The decimation matrix element-by-element can be expressed as:

$$\boldsymbol{D}_{i,j}^{\ell} = \begin{cases} 1, & \text{if } j = iq + (q-1)N\left\lfloor \frac{iq}{N} \right\rfloor + \ell + \left\lfloor \frac{\ell}{q} \right\rfloor (N-q), \\ 0, & \text{otherwise,} \end{cases} \quad (9)$$

where $i = 0,1,\cdots,\frac{N^2}{q^2}-1$, $j=0,1,\ldots,N^2-1$, and $\ell = 0,1,\ldots,q^2-1$.

Figure 6 depicts the downsampling matrix $\mathbf{D}^{\ell}$ for q=2, N=6, and $\ell = 0,1,2,3$. The white squares represent one-valued elements.

In this case, the complete set of measurements is given by

$$\boldsymbol{y} = \begin{bmatrix} \boldsymbol{y}^0 \\ \boldsymbol{y}^1 \\ \vdots \\ \boldsymbol{y}^{q^2-1} \end{bmatrix} = \begin{bmatrix} \boldsymbol{D}^0 \\ \boldsymbol{D}^1 \\ \vdots \\ \boldsymbol{D}^{q^2-1} \end{bmatrix} \mathbf{H}\boldsymbol{f} = \mathbf{H}_S \boldsymbol{f}, \quad (10)$$

where subjacent data cube projection is reconstructed solving an l_1 and l_2 minimization problem, where the decimation process is taken into account. The optimization problem is given by $\tilde{\boldsymbol{f}} = \boldsymbol{\Psi}(\underset{\boldsymbol{\theta}}{\operatorname{argmin}} \|\boldsymbol{y} - \mathbf{H}_S\boldsymbol{\Psi}\boldsymbol{\theta}\|_2 + \tau\|\boldsymbol{\theta}\|_1)$, where $\boldsymbol{y}$ is given by (10), $\mathbf{H}_S$ is the measurement matrix defined as $\mathbf{H}_S = [(\mathbf{D}^0)^T \ldots (\mathbf{D}^{q^2-1})^T]^T \mathbf{H}$, $\boldsymbol{\theta}$ is an S-sparse representation of a low resolution version of $\boldsymbol{f}$ on the basis $\boldsymbol{\Psi}$, and τ is a regularization constant [12].

$\mathbf{H}_S$ is the measurement matrix defined as $\mathbf{H}_S = [(\mathbf{D}^0)^T \ldots (\mathbf{D}^{q^2-1})^T]^T \mathbf{H}$, where $\mathbf{D}^{\ell}$ is the ℓ^{th} downsampling matrix used for measurement selection, $\boldsymbol{\theta}$ is an S-sparse representation of a low resolution version of $\boldsymbol{f}$ on the basis $\boldsymbol{\Psi}$, and τ is a regularization constant.

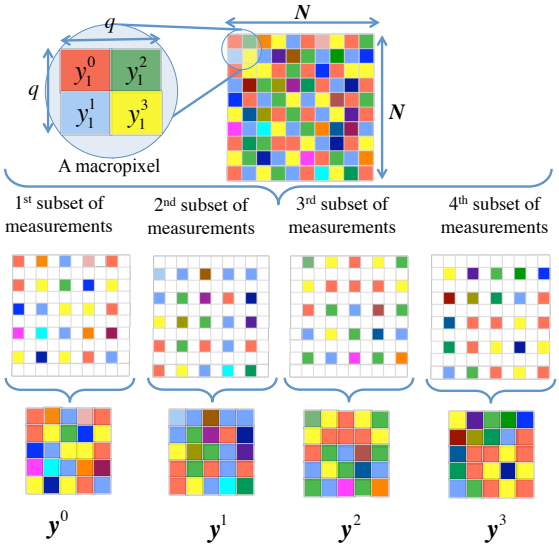

Figure 5. Example of a subset selection for a macropixel size of $q \times q$ = 2×2 that forms 4 subsets of measurements in a single shot of the MSFA-based sensor.

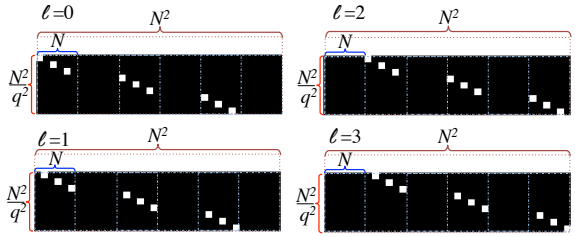

Figure 6. The downsampling matrix $\mathbf{D}^{\ell}$ is shown for q=2, N=6 and $\ell = 0,1,2,3$. White squares represent ones and the black elements are zero.

V. MULTISPECTRAL FILTERS

For developing this work random dichroic filters were used. Dichroic filters let pass only one spectral band for each sensor pixel. Then, the spectral response for pixel can be selected randomly from a set of spectral bands. The spectral response of the (λ_i^D) dichroic filter pixel can be defined as

$$(\mathbf{t}_k)_i = \begin{cases} 1, & \text{if } k = \lambda_i^D, \\ 0, & \text{otherwise,} \end{cases} \quad (12)$$

for the random variable $\lambda_i^D \in \{0,\ldots,L-1\}$, the i^{th} filter where i=0,…,N^2-1, and k=0,…,L-1. For example, the first pixel of a MSFA of L=5 spectral bands can have the spectral response $(\mathbf{t}_k)_1$=[0 1 0 0 0], where the random variable is $\lambda_i^D = 2$.

VI. SIMULATION AND RESULTS

To verify the macropixel CS reconstruction of spectral images sensed by MSFA-based sensors, a set of compressive measurements is simulated using the model of (2). These measurements are constructed employing the Beads spectral image captured with a CCD camera Apogee Alta U260 and a VariSpec liquid crystal tunable filter, in the range of wavelength 400nm-560nm, with steps of 10nm [13]. The resulting test data cube $\mathbf{F}$ has 512×512 pixels of spatial resolution and L=16 spectral bands. The RGB image mapped version of the data cube is shown in Figure 7. An ensemble of dichroic filters based on a random selection of spectral bands is used. Compressive sensing reconstruction is realized using the GPSR algorithm [14]. The representation basis $\boldsymbol{\Psi}$ is a Kronecker product $\boldsymbol{\Psi}=\boldsymbol{\Psi}_1 \otimes \boldsymbol{\Psi}_2$, where $\boldsymbol{\Psi}_1$is the two-dimensional-wavelet Symmlet-8 basis and $\boldsymbol{\Psi}_2$ is the cosine basis. The simulations are performed in a desktop architecture with an Intel Core i7 3.6GHz processor, 32GB RAM, and using Matlab R2014a.

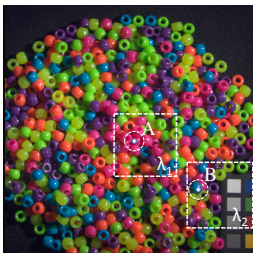

Figure 7. Multispectral image Beads used in simulations (false RGB color).

 ISBN: 978-1-61208-426-8

A. *Variation of the macropixel side size q*

Figure 8 depicts the PSNR of the reconstructed images as a function of the macropixel side size q, for $q \in \{1,2,4,8\}$. Figure 8(a) shows the results when L=3 spectral bands are sensed and reconstructed. Figure 8(b) for L=8, Figure 8(c) for L=12, and Figure 8(d) for L=16. The PSNR comparison is made between the reconstructed image and a spatial decimated version (of size $N/q \times N/q \times L$) of the test data cube. Results show that increasing spectral bands decreases the PSNR for both reconstruction methods. Furthermore, increasing the size of q improves the macropixel CS reconstruction results more than the traditional demosaicing results.

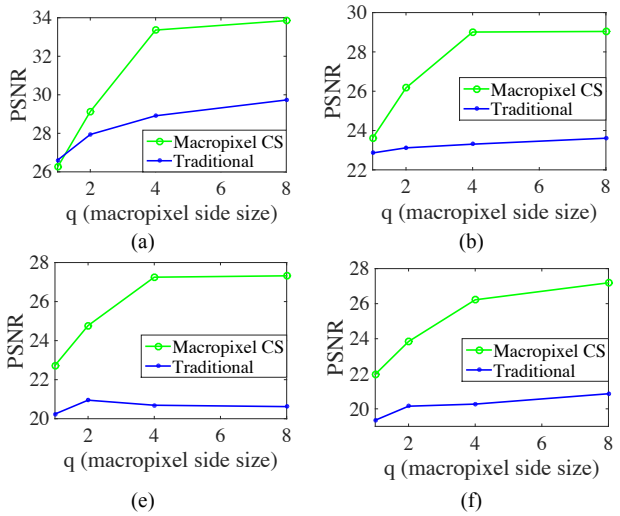

Figure 8. Mean PSNR of the reconstructed data cubes as a function of the macropixel side size q, where L spectral bands are sensed and reconstructed, for (a) L=3, (b) L=8, (c) L=12, and (d) L=16.

Figure 9(a) shows a zoomed version of a selected region of the original 2nd spectral band (this region is highlighted in Figure 7 where λ_1=2). Figure 9 (b) shows its reconstruction when the first L=3 spectral bands are sensed and reconstructed using the macropixel CS approach for q=1. Figure 9(c) illustrates its reconstruction for the traditional demosaicing method. Figure 9(d) depicts reconstruction along the spectral axis of the spatial pixel location A of the Figure 7, where the intensity is normalized between 0-1. Figure 9 (e)-(h) show similar results for the 3rd spectral band and the second region highlighted in Figure 8 for λ_2=3. There, it is possible to observe for L=3 spectral bands the traditional demosaicing has a comparable performance with the macropixel CS reconstruction (around 26 dB in PSNR for both approaches) for q=1 macropixel side size.

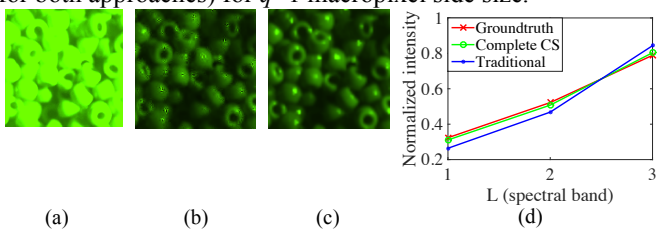

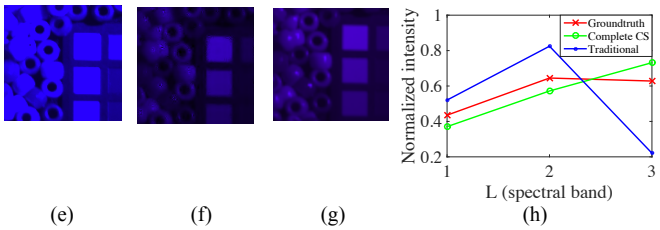

Figure 9. Zoom version of the reconstructions results when L=3 spectral bands are sensed and reconstructed, for q=1. For the spectral band λ_1=2: (a) groundtruth, (b) reconstruction by macropixel CS, (c) reconstruction by a traditional approach, and (d) reconstruction along the spectral axis of the spatial pixel location A in the Fig. 8. For the spectral band λ_2=3: (e) groundtruth, (f) reconstruction by macropixel CS, (g) reconstruction by a traditional approach, and (h) reconstruction along the spectral axis of the spatial pixel location B of the Fig. 8.

Figure 11 shows similar result to those of Figure 10 for q=4, and L=3. Also, in this case it is possible to observe the better performance of the macropixel CS approach where a PSNR improvement of up to 4 dB is attained for q=4 macropixel side size compared with the traditional approach.

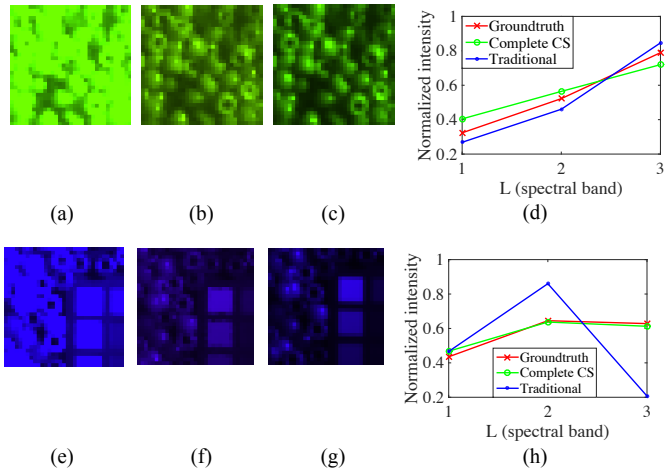

Figure 10. Zoom version of the reconstructions results when L=3 spectral bands are sensed and reconstructed, for q=4. For the spectral band λ_1=2: (a) groundtruth, (b) reconstruction by macropixel CS, (c) reconstruction by a traditional approach, and (d) reconstruction along the spectral axis of the spatial pixel location A in the Fig. 8. For the spectral band λ_2=3: (a) groundtruth, (b) reconstruction by macropixel CS, (c) reconstruction by a traditional approach, and (d) reconstruction along the spectral axis of the spatial pixel location B in the Fig. 8.

Figure 12 (a) shows the selected region of the original 3rd spectral band (in Figure 7 where λ_1=3). Figure 12 (b) shows its reconstruction when the first L=8 spectral bands are sensed and reconstructed using the macropixel CS approach for q=1. Figure 12 (c) illustrates its reconstruction for the traditional demosaicing method. Figure 12 (d) depicts reconstruction along the spectral axis for location A. Figure 12 (e)-(h) show similar results for the 8th spectral band and the second region highlighted in Figure 8 for λ_2=8. The performance of the macropixel CS approach has a PSNR improvement of up to 2 dB for q=1 macropixel side size compared with the traditional demosaicing approach.

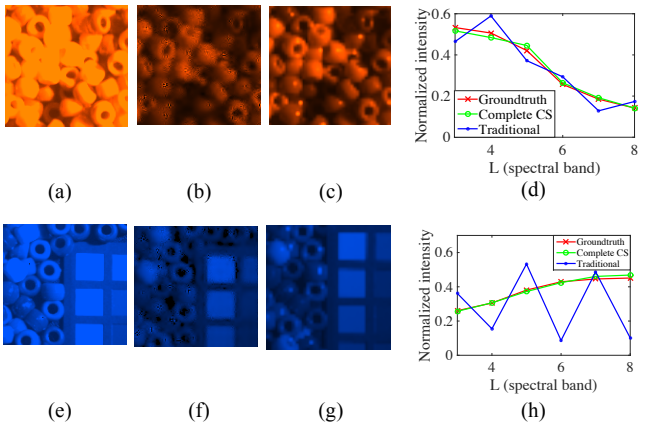

Figure 11. Zoom version of the reconstructions results when L=8 spectral bands are sensed and reconstructed. For the spectral band λ_1=3: (a) groundtruth, (b) reconstruction by macropixel CS for q=1, (c) reconstruction by a traditional approach, and (d) reconstruction along the spectral axis of the spatial pixel location A of the Fig. 8. For the spectral band λ_2=8: (a) groundtruth, (b) reconstruction by macropixel CS for q=1, (c) reconstruction by a traditional approach, and (d) reconstruction along the spectral axis of the spatial pixel location B of the Fig. 8.

Figure 13 shows similar result to those of Figure 12 for q=4, and L=8. Also, it is possible to observe the better performance of the macropixel CS approach where a PSNR improvement of up to 5.7 dB is attained for q=4 macropixel side size compared with the traditional approach. For all cases the macropixel CS approach has a better spectral signature reconstruction than the traditional demosaicing.

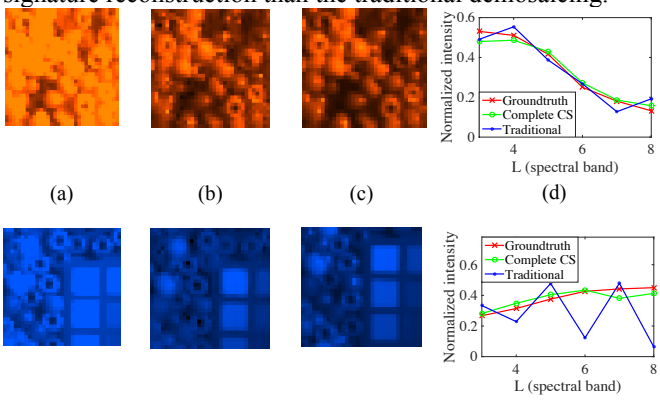

Figure 12. Zoom version of the reconstructions results when L=8 spectral bands are sensed and reconstructed, for q=4. For the spectral band λ_1=3: (a) groundtruth, (b) reconstruction by macropixel CS, (c) reconstruction by a traditional approach, and (d) reconstruction along the spectral axis of the spatial pixel location A in the Fig. 8. For the spectral band λ_2=8: (a) groundtruth, (b) reconstruction by macropixel CS, (c) reconstruction by a traditional approach, and (d) reconstruction along the spectral axis of the spatial pixel location B in the Fig. 9.

VII. CONCLUSION

A model for macropixel CS reconstruction of spectral images sensed by MSFA-based sensors is presented. A selection of measurements subsets to form macropixels that have spectral information of a single reconstructed pixel is exposed. The macropixel CS reconstruction approach is compared with a traditional least squares reconstruction. For the macropixel CS reconstruction, the PSNR increases rapidly with the macropixel side size. For instance, the improvements range from 1 dB to 6 dB with respect to the traditional approach. Results show that increasing spectral bands decreases the PSNR for both reconstruction methods.

REFERENCES

[1] J. Ryan, C. Davis, N. Tufillaro, R. Kudela, and B.-C. Gao, "Application of the Hyperspectral Imager for the Coastal Ocean to Phytoplankton Ecology Studies in Monterey Bay, CA, USA," Remote Sens., vol. 6, no. 2, Jan. 2014, pp. 1007–1025.

[2] Z. Xiong, A. Xie, D.-W. Sun, X.-A. Zeng, and D. Liu, "Applications of Hyperspectral Imaging in Chicken Meat Safety and Quality Detection and Evaluation: A Review.," Crit. Rev. Food Sci. Nutr., Apr. 2014, pp. 1287-1301.

[3] G. J. Bellante, S. L. Powell, R. L. Lawrence, K. S. Repasky, and T. a. O. Dougher, "Aerial detection of a simulated CO2 leak from a geologic sequestration site using hyperspectral imagery," Int. J. Greenh. Gas Control, vol. 13, Mar. 2013, pp. 124–137.

[4] M. Mehrübeoglu, G. W. Buck, and D. W. Livingston, "Differentiation of bacterial colonies and temporal growth patterns using hyperspectral imaging," in SPIE Optical Engineering + Applications, 2014, p. 922206.

[5] G. Lu and B. Fei, "Medical hyperspectral imaging: a review.," J. Biomed. Opt., vol. 19, no. 1, Jan. 2014, p. 10901.

[6] J. D. Barrie, K. a. Aitchison, G. S. Rossano, and M. H. Abraham, "Patterning of multilayer dielectric optical coatings for multispectral CCDs," Thin Solid Films, vol. 270, no. 1–2, Dec. 1995, pp. 6–9.

[7] Z. Frentress, L. C. Young, and H. D. Edwards, "Field Photometer with Nine-Element Filter Wheel," Appl. Opt, vol. 3, 1964, pp. 303–309.

[8] P. J. Lapray, X. Wang, J. B. Thomas, and P. Gouton, "Multispectral Filter Arrays: Recent Advances and Practical Implementation," Sensors, vol. 14, 2014, pp. 21626–21659.

[9] L. Miao, H. Qi, R. Ramanath, and W. E. Snyder, "Binary tree-based generic demosaicking algorithm for multispectral filter arrays," IEEE Trans. Image Process., vol. 15, no. 11, 2006, pp. 3550–3558.

[10] J. Brauers and T. Aach, "A Color Filter Array Based Multispectral Camera," 12 Work. Farbbildverarbeitung, 2006.

[11] Y. Monno, M. Tanaka, and M. Okutomi, "Multispectral Demosaicking Using Adaptive Kernel Upsampling," in In Proceedings of the 18th IEEE International Conference on Image Processing (ICIP), 2011, pp. 3218–3221.

[12] H. Arguello and G. R. Arce, "Colored coded aperture design by concentration of measure in compressive spectral imaging.," IEEE Trans. Image Process., vol. 23, no. 4, Apr. 2014, pp. 1896–908.

[13] S. K. N. F. Yasuma, T. Mitsunaga, and D. Iso, "CAVE | Projects: Multispectral Image Database," Generalized Assorted Pixel Camera: Post-Capture Control of Resolution, Dynamic Range and Spectrum. [Online]. Available: http://www.cs.columbia.edu/CAVE/databases/multispectral/. [Accessed: 24-Feb-2015].

[14] M. A. Figueiredo, R. D. Nowak, and S. J. Wright, "Gradient projection for sparse reconstruction: Application to compressed sensing and other inverse problems.," Sel. Top. Signal Process. IEEE J., vol. 1, no. 4, 2007, pp. 586–597.

 ISBN: 978-1-61208-426-8